



Improvement of stability of sinusoidally driven atmospheric pressure plasma jet using auxiliary bias voltage

Hyun-Jin Kim, Jae Young Kim, Jae Hyun Kim, Dong Ha Kim, Duck-Sik Lee, Choon-Sang Park, Hyung Dal Park, Bhum Jae Shin, and Heung-Sik Tae

Citation: [AIP Advances](#) **5**, 127141 (2015); doi: 10.1063/1.4939577

View online: <http://dx.doi.org/10.1063/1.4939577>

View Table of Contents: <http://scitation.aip.org/content/aip/journal/adva/5/12?ver=pdfcov>

Published by the [AIP Publishing](#)

Articles you may be interested in

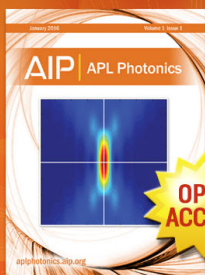
[On the use of the double floating probe method to infer the difference between the electron and the heavy particles temperatures in an atmospheric pressure, vortex-stabilized nitrogen plasma jet](#)
Rev. Sci. Instrum. **85**, 053507 (2014); 10.1063/1.4875215

[Are all atmospheric pressure cold plasma jets electrically driven?](#)
Appl. Phys. Lett. **100**, 123702 (2012); 10.1063/1.3696889

[Atmospheric pressure argon plasma jet using a cylindrical piezoelectric transformer](#)
Appl. Phys. Lett. **95**, 211501 (2009); 10.1063/1.3267142

[Experimental investigation of dielectric barrier discharge plasma actuators driven by repetitive high-voltage nanosecond pulses with dc or low frequency sinusoidal bias](#)
J. Appl. Phys. **104**, 043304 (2008); 10.1063/1.2968251

[Study of Electrokinetic Effects Using Sinusoidal Pressure and Voltage](#)
J. Chem. Phys. **23**, 2299 (1955); 10.1063/1.1740742



Launching in 2016!
The future of applied photonics research is here

AIP | APL
Photonics

Improvement of stability of sinusoidally driven atmospheric pressure plasma jet using auxiliary bias voltage

Hyun-Jin Kim,¹ Jae Young Kim,² Jae Hyun Kim,¹ Dong Ha Kim,¹
 Duck-Sik Lee,¹ Choon-Sang Park,¹ Hyung Dal Park,³ Bhum Jae Shin,⁴
 and Heung-Sik Tae^{1,a}

¹*School of Electronics Engineering, College of IT Engineering, Kyungpook National University, Daegu, 702-701, Korea*

²*Department of New Biology, Daegu Gyeongbuk Institute of Science & Technology, Daegu 711-873, Korea*

³*Department of Mechanical Equipment Development, Radiation Technology eXcellence, Daejeon 305-353, Korea*

⁴*Department of Electronics Engineering, Sejong University, Seoul 143-747, Korea*

(Received 13 October 2015; accepted 22 December 2015; published online 31 December 2015)

In this study, we have proposed the auxiliary bias pulse scheme to improve the stability of atmospheric pressure plasma jets driven by an AC sinusoidal waveform excitation source. The stability of discharges can be significantly improved by the compensation of irregular variation in memory voltage due to the effect of auxiliary bias pulse. From the parametric study, such as the width, voltage, and onset time of auxiliary bias pulse, it has been demonstrated that the auxiliary bias pulse plays a significant role in suppressing the irregular discharges caused by the irregular variation in memory voltage and stable discharge can be initiated with the termination of the auxiliary bias pulse. As a result of further investigating the effects of the auxiliary pulse scheme on the jet stability under various process conditions such as the distance between the jet head and the counter electrode, and carrier gas flow, the jet stability can be improved by adjusting the amplitude and number of the bias pulse depending on the variations in the process conditions. © 2015 Author(s). All article content, except where otherwise noted, is licensed under a Creative Commons Attribution 3.0 Unported License. [<http://dx.doi.org/10.1063/1.4939577>]

I. INTRODUCTION

The atmospheric pressure plasma jet (APPJ) has been intensively studied for various applications such as biomedical application, surface modification, nanostructure fabrication, and polymerization.^{1–8} Various APPJs generated using different power supply schemes have demonstrated remarkable results in a variety of applications.^{9–11} Among them, APPJ driven by sinusoidal wave (SW-APPJ) with combination of the dielectric barrier is widely used for heat-sensitive biomedical application, because it can be easy to generate low temperature plasma at atmospheric pressure by utilizing the current limiting features of the dielectric barrier.^{1–6} However, the SW-APPJ with combination of the dielectric barrier shows worse stability (*i.e.*, cycle-to-cycle reproducibility) which limits practical applications.^{12–14} Accordingly, several groups have reported that the stability problem in sinusoidal operation of atmospheric pressure dielectric barrier discharges (DBDs) was strongly related with the surface charges accumulated on the dielectric plates during a plasma discharge.^{14–20} Furthermore, many research groups have studied on what kinds of parameters aggravate a stable production of the atmospheric pressure plasma, thereby reporting that a worse stability of the SW-APPJ is inherently caused by the irregular variation in the charge accumulation depending on the applied voltage and frequency.^{12–20} In other words, the firing condition of the SW-APPJ strongly depends on the gap voltage between two electrodes, which is determined by the sum of the externally applied voltage

^aAuthor to whom correspondence should be addressed; electronic mail: hstae@ee.knu.ac.kr



and the voltage internally induced by the accumulated charges (*i.e.* memory voltage).^{16–18} Therefore, suppressing the irregular variation in memory voltage is a key factor for improving the stability of the SW-APPJ applicable to industrial fabrication processes.

Our experimental results will show that by properly applying the auxiliary bias pulse to the counter electrode, it is possible to suppress the irregular discharges caused by the variation in memory voltage, thereby resulting in obtaining the improved stability of the SW-APPJ. In this study, we have measured the memory voltage determined by the variation of the surface charges accumulating on the dielectric barrier of the counter electrode of the SW-APPJ, showing that the abrupt variations in the memory voltage can affect the ensuing discharge considerably. Accordingly, we employ the auxiliary bias pulse cooperated with sinusoidal waveform, which is additionally applying to the counter electrode, in order to suppress the abrupt variation in the memory voltage. In particular, we examine carefully the effects of three parameters such as the width, voltage, and onset time of the auxiliary bias pulse on the improvement of the stability of SW-APPJ. Furthermore, we examine the effects of the bias pulse scheme on the jet stability as variations of the process parameters such as the distance between the jet head and the counter electrode and the gas flow rate by applying the various bias pulses with different amplitudes and numbers to the counter electrode.

II. EXPERIMENTAL

Figure 1 shows a schematic diagram of the experimental setup employed in this study. As shown in Fig. 1(a), the atmospheric pressure plasma jet is comprised of a needle-type powered electrode and external plate-type counter electrode, where the needle electrode is apart from a jet head at a distance of 10 mm. A copper wire with a diameter of 0.5 mm is used as a powered electrode and coaxially located inside a quartz tube with an inner diameter (ID) of 2 mm and outer diameter (OD) of 3 mm. The distance between the jet head and the indium tin oxide (ITO) coated glass with a thickness of 1.2 mm is varied from 5 to 15 mm, thus serving as the counter electrode in which the glass side faces the plasma jet. Argon gas (UHP grade; 99.999 %) is used as the discharge gas and its flow is also varied from 2000 to 5000 sccm (standard cubic centimeters per minute).

The sinusoidal waveform with a frequency of 25 kHz, generated by a high-voltage (HV) amplifier, is applied to the powered electrode. The auxiliary bias pulse synchronized with the sinusoidal waveform is generated by a biasing circuit with a function generator. As a main experiment, the bias pulse is additionally applied to the counter electrode for improving the discharge stability, as shown in Fig. 1(a). Since the auxiliary bias pulse is applied to the counter electrode during application of the positive-going sinusoidal waveform, the applied voltage between the powered and counter electrode

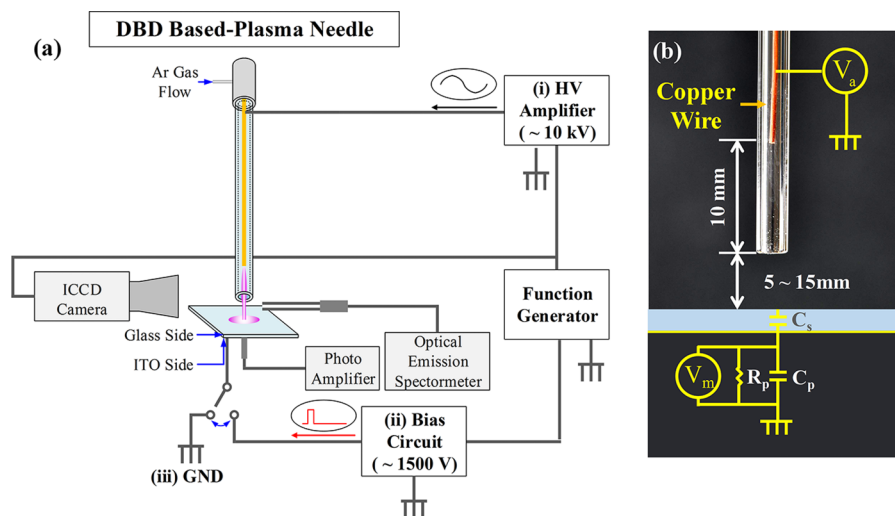


FIG. 1. Schematic diagram of experimental setup employed in this study (a) and measurement set-up to investigate variations in memory voltages (b).

is reduced. Accordingly, the objective of the auxiliary bias pulse is suppressing the initial firing condition of APPJs by reducing the effective applied voltage between the powered and counter electrode. The voltage and current waveforms are measured using a high-voltage probe (Tektronix P6015A) and current probe (Pearson 4100), respectively. A photo-sensor amplifier (Hamamatsu C6386-01), covering a wavelength range of 550 - 1000 nm, is also used to measure the optical emissions from Ar plasma. The voltage, current, and optical emission waveforms are plotted on an oscilloscope (Lecroy WaveRunner 64 Xi). The discharge images under various gas flow rates are measured using an intensified charge-coupled device (ICCD) camera (Princeton Instruments, PI-MAX II) with an exposure time of 40 ms in the shutter mode. To investigate the changes of the resultant excited species in ambient air depending on whether the bias pulse is applied or not, the optical emission spectroscopy (OES) is measured at the five points from the jet head to the couther electrode with an interval of 2 mm using a fiber optic spectrometer (Ocean Optics, USB4000). A 10 mm-long alumina tube with an inner diameter (ID) of 2 mm is mounted to an optical probe tip with a focal lens in order to enhance the resolution of spatial distribution of plasma plume.

To investigate the variation of surface charges accumulating on the dielectric barrier of the counter electrode, the measurement set-up is employed, as shown in Fig. 1(b). Since it is difficult to directly measure the variation in surface charges on the counter electrode, the voltage variation on the ITO side of the counter electrode is measured using a high-voltage probe (Tektronix P6015A) with a input resistance ($R_p = 100 \text{ M}\Omega$) and capacitance ($C_p = 3 \text{ pF}$). The memory voltage (V_m), which is charged by the discharge to the capacitor of the high-voltage probe, is obtained by subtracting the measured voltage of discharge-off condition from the values of the discharge-on condition. Therefore, the memory voltage V_m can be regarded as an indicator of the variation of surface charges accumulating on the dielectric barrier of the counter electrode.

III. RESULTS AND DISCUSSION

Figure 2 shows the time evolutions of the memory voltage V_m and corresponding optical emissions driven by sinusoidal waveform of 4.75 kV at a frequency of 15 kHz. In Fig. 2, the distance between the jet head and the counter electrode is 5 mm and the gas flow rate is 500 sccm. As shown in Fig. 2(a), from $t = -500$ to $t = 100 \mu\text{s}$, the discharges rather stably occur. Accordingly, the variations of optical emissions and memory voltages are relatively small. However, as shown in the irregular discharge region of Fig. 2(a), the abruptly changed optical emissions are strongly related to the variations of memory voltage. In order to further investigate the correlation between the optical emission and the modified memory voltage, the irregular discharge region, which is marked in Fig. 2(a), is magnified in Figs. 2(b) and 2(c).

Since the discharge can start in the case of applying the gap voltage greater than the firing voltage between two electrodes, the internal memory voltage V_m set up during the previous discharge can have a significant influence on when the subsequent discharge is initiated especially in the SW-APPJ. As shown in Figs. 2(b) and 2(c), the discharges are produced three times during each period. During the 1st period, the weak discharge is produced due to the low applied voltage between the powered and counter electrode. In this situation, the memory voltage is changed relatively low, as shown in Fig. 2(b). The following 2nd and 3rd discharges are strongly produced and corresponding memory voltage variations are also significantly changed. However, the 3rd discharge (i) during the 3rd period is produced earlier than the previous discharges, thereby resulting in reducing the memory voltage due to the reduced voltage applied between the powered and counter electrodes. Consequently, during the 4th period, the production of ensuing discharge (ii) is delayed due to the lowered memory voltage induced by the previous weak discharge. Nonetheless, the ensuing second discharge (iii) shows the increased optical intensity and memory voltage due to the increased applied voltage, as shown in (iii) of Fig. 2(c). Finally, the discharge (iv) is earlier produced due to the increased memory voltage induced by the previous discharge. These results indicate that the stability of discharge is strongly related to the variation of memory voltage. Therefore, in order to improve the stability of discharge, it is important to minimize the variation of memory voltage.

Figure 3(a) shows the overlapped optical emissions with 25 times, when the sinusoidal waveform of 2.5 kV at a frequency of 25 kHz is applied without the auxiliary bias pulse. In Fig. 3, the distance

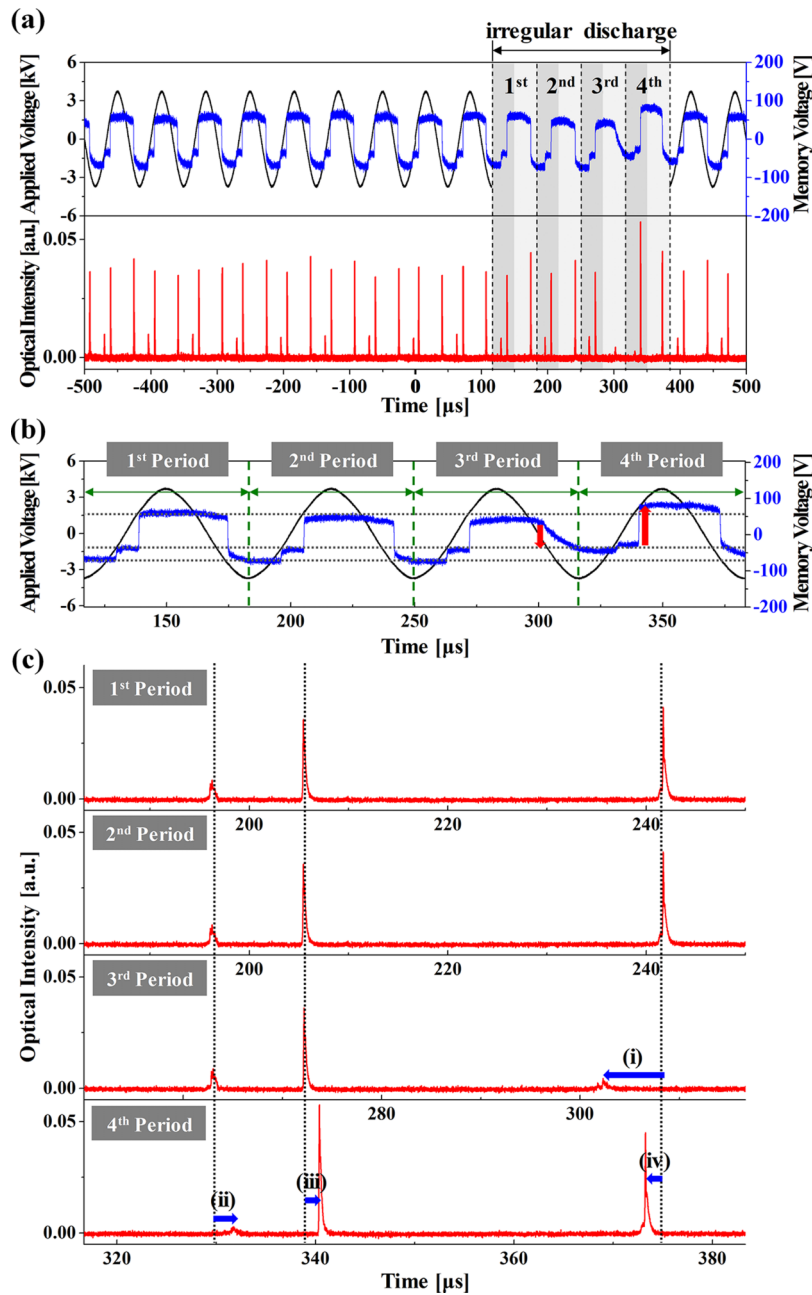


FIG. 2. Time evolutions of memory voltages and corresponding optical emissions when sinusoidal waveform of 4.75 kV is applied without auxiliary bias pulse (a), memory voltages (b) measured during four periods in irregular discharge of (a), and corresponding optical emissions (c) measured during four periods in irregular discharge of (a).

between the jet head and the counter electrode and gas flow rate are exactly the same as those of Fig. 2, respectively. As shown in Fig. 3(a), the optical emissions are distributed from 0 to 4.5 μs , which illustrates the production of irregular discharges. Since the sinusoidal waveform has a slow voltage slope, the ignition voltage of sinusoidal waveform is strongly dependent on the variation of memory voltage induced by the previous discharge. Therefore, these irregular discharges are mainly related to the variation of memory voltage. It would be a major reason for inducing the discharge instability in the case of applying the sinusoidal waveform.

Accordingly, this study proposes the auxiliary bias pulse scheme cooperated with sinusoidal waveform, which is additionally applying the bias pulse to the counter electrode to compensate the

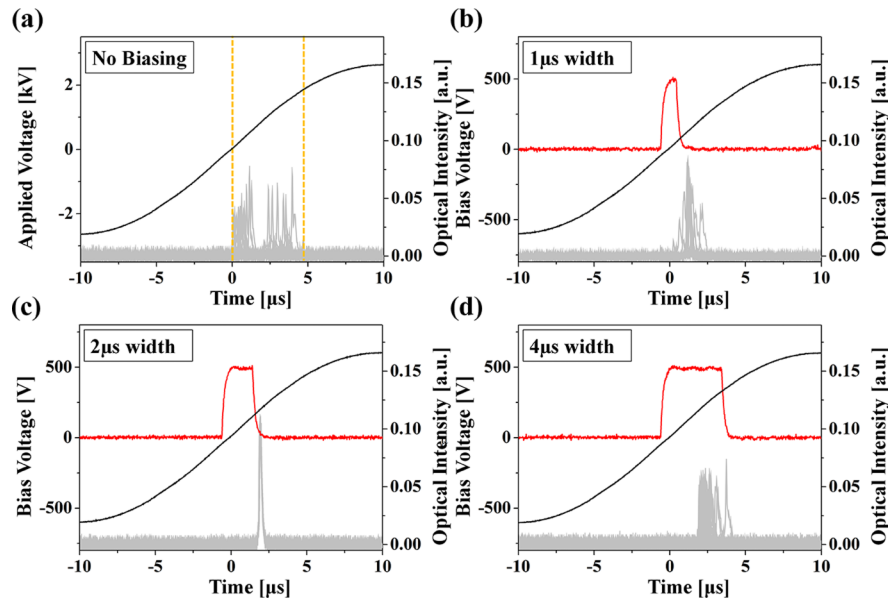


FIG. 3. Overlapped optical emissions measured under various auxiliary bias pulse conditions when sinusoidal waveform of 2.5 kV is applied: (a) without auxiliary bias pulse, (b) with auxiliary bias pulse width of 1 μ s, (c) with auxiliary bias pulse width of 2 μ s, and (d) with auxiliary bias pulse width of 4 μ s.

variation of memory voltage. The basic idea of the auxiliary bias pulse scheme is to suppress the irregular discharge by reducing the gap voltage with the bias pulse. When the bias pulse is applied to the counter electrode, the gap voltage is abruptly reduced because the polarity of the bias pulse is the same as that of the sinusoidal waveform. Therefore, the gap voltage cannot reach the ignition voltage, thereby resulting in suppressing the irregular discharges during the applying of bias pulse. Furthermore, when the application of the bias pulse is terminated, the discharge can stably initiate due to the satisfaction of ignition condition.

Figures 3(b), 3(c), and 3(d) show the overlapped optical emissions related to the bias pulse width when the bias pulse of 500 V is applied at $t = -0.5$ μ s. As shown in Fig. 3(c), when the bias pulse width is 2 μ s, it should be noted that the irregular discharge is suppressed during the application of bias pulse and the stable discharge is initiated immediately after termination of the bias pulse. Since the cycle-to-cycle variation in memory voltage is gradually decreased due to the effect of the bias pulse, the width of the bias pulse is less than that of the initial variation of memory voltage. However, as shown in Fig. 3(b), when the bias pulse width (= 1 μ s) is insufficient to compensate the variation of memory voltage, the irregular discharges are observed to still occur after termination of the bias pulse. Furthermore, as shown in Fig. 3(d), when the bias pulse width (= 4 μ s) is too long, the irregular discharge is observed to occur even during the application of bias pulse.

Figure 4(a) shows the measured optical emission peaks during the application of the positive-going sinusoidal waveform when applying optical various bias pulses with different onset times. In the bias pulses applied in Fig. 4(a), their widths and voltages are fixed at 2 μ s and 500 V, respectively, whereas their onset times ($= T_{B_ON}$) are shifted from -0.5 to -2.0 μ s at an interval of 0.5 μ s. As shown in Fig 4(a), no discharge is produced during the application of each bias pulse, and optical emission peaks are observed immediately after the application period of bias pulse is terminated. Furthermore, it is observed that the corresponding optical intensity is increased as the onset time of the bias pulse is shifted from -2.0 to -0.5 μ s. The increase in the optical emission intensity with respect to the shift of the onset time of bias pulse is mainly due to the increased applied voltage.

Figure 4(b) shows the optical emissions measured during the successive 25 periods of the sinusoidal waveform when adopting the various bias pulses of Fig. 4(a) including no bias pulse condition. At no bias pulse condition, irregular optical emission peaks are observed during overall period, which is confirmed from the experimental result of the overlapped optical emissions peaks distributed from 0 to 4.5 μ s in Fig 3(a). However, when the bias pulse is applied to the counter electrode, the irregular

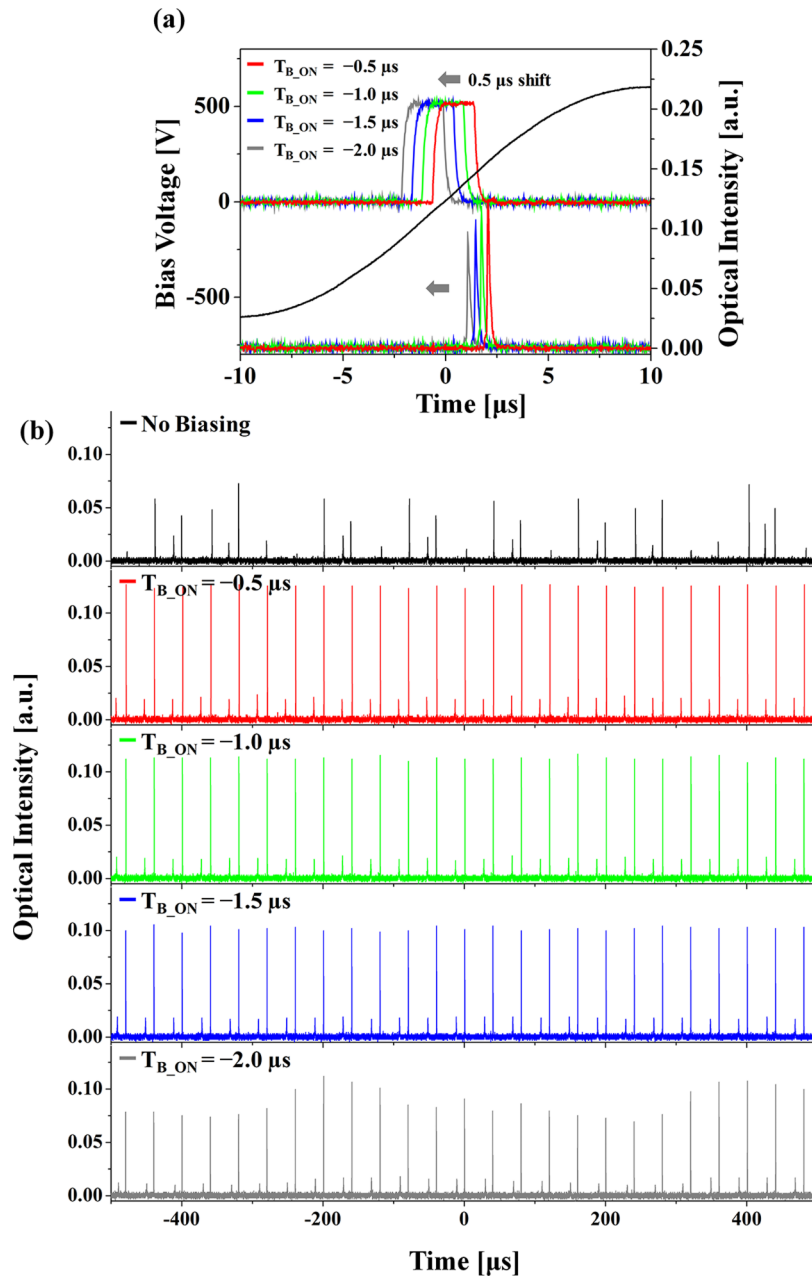


FIG. 4. Measured optical emissions (a) during half period of sinusoidal waveform of 2.5 kV under four different onset times ($=T_{B_ON}$) of auxiliary bias pulses ranging from -0.5 to $-2.0 \mu s$ at interval of $0.5 \mu s$ but other conditions (pulse width $= 2 \mu s$ and voltage $= 500$ V) are same, and measured optical emissions (b) during successive 25 periods of sinusoidal waveform under same bias pulse condition of (a).

discharges are suppressed for the cases of $T_{B_ON} = -0.5$ to $-1.5 \mu s$, as shown in Fig. 4(b). These experimental results clearly reveal that the stability of discharges for cycle-to-cycle is significantly improved due to the effect of the bias pulse. However, in the case of $T_{B_ON} = -2.0 \mu s$, which does not include duration of the irregular discharges shown in the overlapped optical emissions peaks distributed from 0 to $4.5 \mu s$ in Fig 3(a), the stability of discharge is sharply worsened. Consequently, the experimental results of Figs. 3 and 4 confirm that applying auxiliary bias pulse with proper pulse width and onset time which can effectively suppress the irregular discharge, is very important for improving the stability of SW-APJ. In order to suppress the irregular discharges due to the variation in memory voltage, the application period of the bias pulse needs to include the duration of the irregular

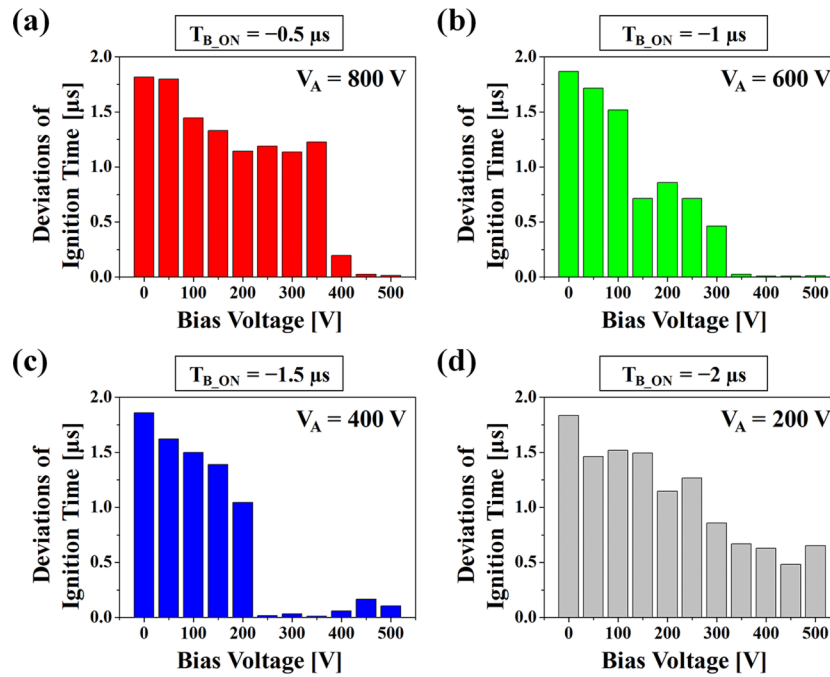


FIG. 5. Standard deviations of ignition times with 300 successive discharges as functions of bias voltage from 0 to 500 V at four different onset times (T_{B_ON}) of auxiliary bias pulses under same experimental conditions of Fig. 4: (a) $T_{B_ON} = -0.5 \mu s$, (b) $T_{B_ON} = -1.0 \mu s$, (c) $T_{B_ON} = -1.5 \mu s$, and (d) $T_{B_ON} = -2.5 \mu s$.

discharges, and the amplitude of the bias pulse needs to be high enough to compensate the variation in memory voltage. However, the voltage levels of bias pulse necessary for suppressing the irregular discharge can vary depending on the onset time of the bias pulse.

Figure 5 shows the standard deviation of ignition time with 300 successive discharges relative to the variations in the bias voltages ranging from 0 to 500 V under the same experimental conditions of Fig. 4. In Fig. 5, the applied voltages, V_A of sinusoidal waveform are measured at the termination time of the application period of bias pulse; $V_A = 800$ V at $t = 1.5 \mu s$ (i.e., $T_{B_ON} = -0.5 \mu s$) in (a), $V_A = 600$ V at $t = 1.0 \mu s$ (i.e., $T_{B_ON} = -1.0 \mu s$) in (b), $V_A = 400$ V at $t = 0.5 \mu s$ (i.e., $T_{B_ON} = -1.5 \mu s$) in (c), and $V_A = 200$ V at $t = 0.0 \mu s$ (i.e., $T_{B_ON} = -2.0 \mu s$) in (d). As the bias voltage increases, the standard deviation of ignition time tends to decrease due to the effect of the bias pulse, meaning that the discharges tend to be produced regularly. In particular, the significant decline in the standard deviation (STD) of ignition time is observed to occur at different bias voltages for different T_{B_ON} . These significant declines in the STD of ignition time occur at the bias voltage of 450 V, 350 V, and 250 V in Figs. 5(a), 5(b) and 5(c), respectively, which indicates that the higher bias voltage is necessary for suppressing the irregular discharges, as the T_{B_ON} is changed from -0.5 to $-1.5 \mu s$. The requirement of the higher bias voltage for suppressing irregular discharge at different onset times ranging from -0.5 to $-1.5 \mu s$ is mainly due to the increase in the applied voltages, V_A of sinusoidal waveform depending on the termination time of the application period of bias pulse. In contrast, in the case of $T_{B_ON} = -2 \mu s$, the standard deviation of ignition time does not significantly decline, even though the bias voltage increases up to 500 V, as shown in Fig. 5(d). This result implies that when the application period of the bias pulse does not include the duration of the irregular discharges, the bias voltage cannot effectively compensate the variation in memory voltage.

From the parametric study of the proposed auxiliary bias pulse scheme, the three following conditions are required to suppress irregular discharges in the SW-APPJ; first, the auxiliary bias pulse is required to have a proper width based on the variation of the memory voltage, second, the application period of the auxiliary bias pulse is required to include a duration of the irregular discharges, and third, the amplitude of the auxiliary bias pulse is required to be determined according to the value of the sinusoidal waveform depending on the application period of the auxiliary bias pulse.

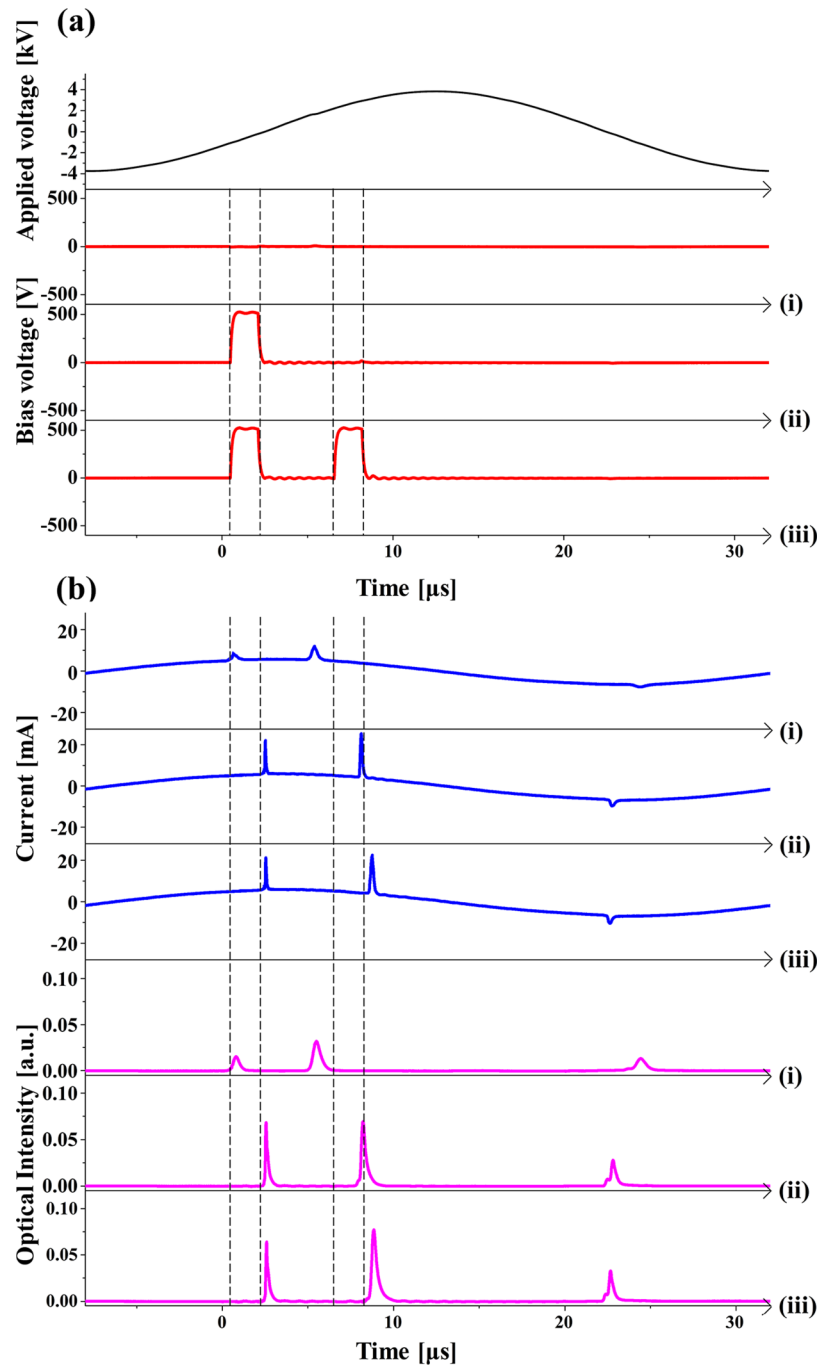


FIG. 6. Averaged waveforms of current and optical emission during 1000 periods when sinusoidal waveform of 3.5 kV is applied at frequency of 25 kHz under different bias pulse conditions, where the distance between jet head and counter ground electrode is 5 mm; (a) applied voltage and three different bias conditions ((i) no bias, (ii) one bias pulse during 1st discharge, and (iii) two bias pulses during 1st and 2nd discharges) and (b) corresponding currents and optical emissions under three different bias pulse conditions such as (i), (ii), and (iii).

Figure 6 shows the averaged waveforms of the current and optical emission during 1000 periods when the sinusoidal waveform of 3.5 kV is applied at a frequency of 25 kHz under different bias pulse conditions, where in (a), sinusoidal and bias voltages ((i) no bias, (ii) one bias pulse during the 1st discharge, and (iii) two bias pulses during the 1st and 2nd discharges) are applied to the powered and counter electrodes, respectively, and in (b), the measured currents and optical emissions under

three different bias pulse conditions are shown. As shown in Fig. 6(b)-(i), when the bias pulse is not applied, discharges are produced twice during the application of the positive-going sinusoidal waveform, and the widths and peaks of the current and optical emission are observed to be wide and low, respectively. Since the waveforms are 1000 times averaged, the widening of the current and optical emissions including low intensity peaks indicate the irregular distribution of the discharge initiations during respective period, *i.e.*, poor stability.

As a result of previous parametric study on the auxiliary bias pulse scheme, the optimized bias pulse is applied during the 1st discharge, as shown in Fig. 6(a)-(ii). Unlike no bias condition in Fig. 6(b)-(i), when the proper bias pulse is applied during the 1st discharge, the current and optical emission of Fig. 6(b)-(ii) illustrate the narrow width with a high peak, which would result from the improved cycle-to-cycle reproducibility. Furthermore, Fig. 6(b)-(ii) also illustrates that the production of the stable discharge during the 1st discharge due to the application of single bias pulse can contribute to producing the successive stable discharges. In addition to the bias condition of Fig. 6(a)-(ii), another bias pulse is additionally applied during the 2nd discharge, in order to investigate the effect of another bias pulse on the 2nd discharge characteristics. As shown in Fig. 6(b)-(iii), the current and optical emission only during the 2nd discharge are observed to be slightly delayed but their widths and peaks are almost the same as those of Fig. 6(b)-(ii). As a consequence of Fig. 6, it is confirmed that the application of single bias pulse during the 1st discharge is sufficient for improving the discharge stability for whole period.

In order to further investigate the effects of auxiliary bias pulse scheme on the jet stability under various process conditions, especially such as the distance between the jet head and counter ground electrode and the gas flow rate, the correlations of the bias pulse conditions to the jet stability are examined. Figures 7(a) and 7(b) show the averaged waveforms of the optical emission during 1000 periods under different bias pulse conditions when the distance ($=d$) between the jet head and counter electrode is larger than 5 mm (*i.e.*, (a) $d=10$ mm and (b) $d=15$ mm). When compared to the applied voltage of Fig. 6 (that is, $d=5$ mm case), the applied voltages of Figs. 7(a) and 7(b) are required to be higher in order to compensate the decreased potential gradient in the gap. As shown in Fig. 7(a)-(i), when the bias pulse is not applied, discharges are produced three times during the application of the positive-going sinusoidal waveform of 4 kV, and the corresponding optical emission peaks show the irregular distribution of the discharge initiations during the respective period. When the bias pulse of 500 V is applied once during the 1st discharge, the irregular distribution of the discharge initiations is improved slightly, as shown in Fig. 7(a)-(i), unlike previous results of Figs. 6(a)-(ii) and 6(b)-(ii). However, by increasing the bias voltage from 500 to 1000V, the optical emissions of the 1st and 2nd discharges are observed to be increased and narrow, as shown in Fig. 7(a)-(iii). In addition, when another bias pulse of 1000 V is additionally applied during the 2nd discharge, the stabilities of the 2nd discharge and successive discharges during the application of the negative-going sinusoidal waveform are also observed to be more enhanced, as shown in Fig. 7(a)-(iv). The experimental result of Fig. 7(a) illustrates that, as the distance between the jet head and counter ground electrode gets more increased, the more severe bias pulse conditions are required to suppress the irregular discharges induced by the decrease in the potential gradient proportional to the increase of the distance between the jet head and counter ground electrode.

When the distance between the jet head and counter ground electrode gets more increased, that is, $d=15$ mm, many irregular discharges are produced at the applied sinusoidal waveform of 6 kV, as shown in no bias condition of Fig. 7(b)-(i). In this process condition, it is observed that when the two bias pulses of 1000 V are applied during the 1st and 2nd discharges like the case of Fig. 7(a)-(iv), the stabilities of the 1st and 2nd discharges are considerably enhanced but the ensuing discharges are still irregularly produced, as shown in Fig. 7(b)-(ii). When the higher pulse voltages of 1500V are applied in the consideration of the increased distance between the jet head and counter ground electrode, the stabilities of the 1st and 2nd discharges are more enhanced and nevertheless the 3rd discharge is not yet stable, as shown in Fig. 7(b)-(iii). In addition to the bias condition of Fig. 7(b)-(iii), third bias pulse is additionally applied during the 3rd discharge, as shown in Fig. 7(b)-(iv), thereby resulting in producing the four stable discharges during the whole period. These results confirm that as the distance between the jet head and counter ground electrode gets more increased, the higher voltage and additional numbers of the bias pulses are required to obtain the jet stability.

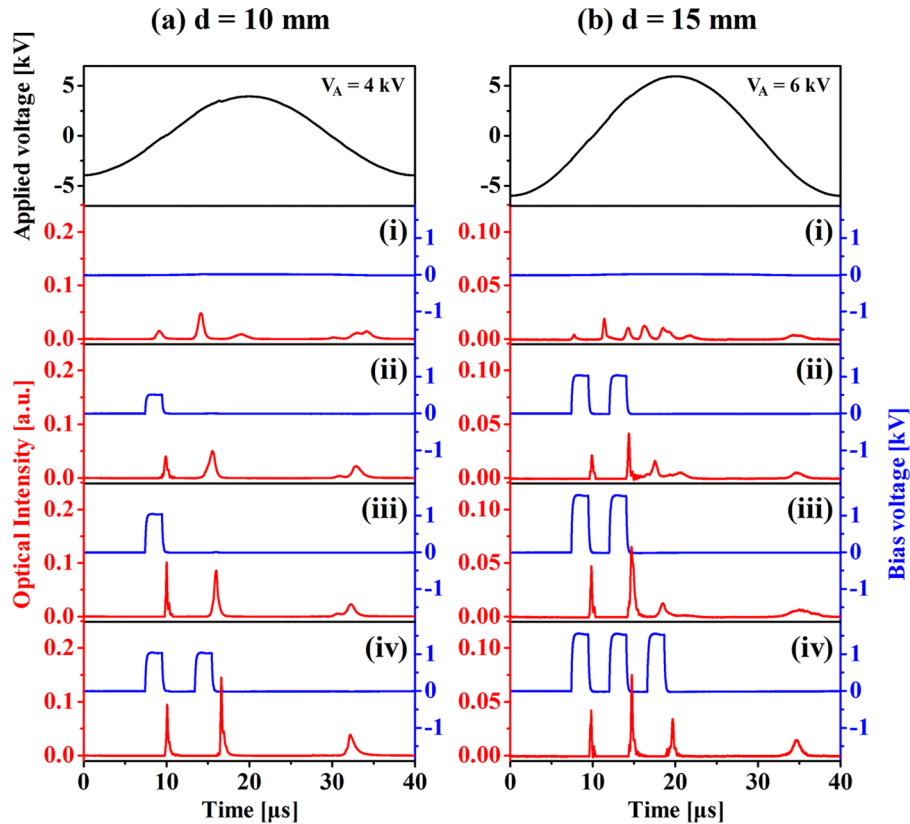


FIG. 7. Averaged waveforms of optical emissions during 1000 periods under different bias pulse conditions when distance ($=d$) between jet head and counter electrode is larger than 5 mm (*i.e.*, (a) $d=10$ mm and (b) $d=15$ mm). Applied sinusoidal waveforms are 4 kV for (a) $d=10$ mm, and 6 kV for (b) $d=15$ mm at frequency of 25 kHz, respectively. Detailed bias pulse conditions are given as follows; in Fig. 7(a), (i) is no bias, (ii) one bias pulse of 500 V during 1st discharge, (iii) one bias pulse of 1000 V during 1st discharge, and (iv) two bias pulses of 1000 V during 1st and 2nd discharges, whereas in Fig. 7(b), (i) is no bias, (ii) two bias pulses of 1000 V during 1st and 2nd discharges, (iii) two bias pulses of 1500 V during 1st and 2nd discharges, and (iv) three bias pulses of 1500 V during 1st, 2nd and 3rd discharges.

To investigate the changes of the jet stability as a function of the gas flow rate, only the gas flow rate are varied from 200 to 600 sccm, but the other process conditions are exactly the same as those of Fig. 7(a)-(i) and (iv). Figures 8(a) and 8(b) show the averaged waveforms of the current and optical emission during 1000 periods relative to the gas flow rate ranging from 200 to 600 sccm without and with the application of the bias pulse of Fig. 7(a)-(iv). Figures 8(c) and 8(d) show the ICCD images of the discharges produced under the process conditions of Figs. 8(a) and 8(b), respectively. These discharge images of Figs. 8(c) and 8(d) are obtained by accumulating all discharges produced during 1000 periods ($=40$ ms) with an intensified charge coupled device (ICCD) camera. When the bias pulse is not applied in Fig. 8(a), *i.e.*, ground counter electrode condition, the distributions of the discharge initiations are observed to change considerably depending on the variation of the gas flow rate, as shown in Fig. 8(a). At the gas flow rate of 200 sccm, the plasma plume does not extend from the jet head toward the ground counter electrode, as shown in the ICCD image of Fig. 8(c)-(i), which would be presumably due to an insufficient carrier gas supply toward surrounding air. Thus the spatial distribution of optical emission sharply decreases in the vicinity of the jet head, as depicted in Fig. 8(c)-(i), and as such the space charge distributions would be expected to decrease sharply near the jet head from the observation of the ICCD images of Fig. 8(c)-(i). In this case, the optical emissions are very weak during the application of the positive-going sinusoidal waveform and are hardly observed during the application of the negative-going sinusoidal waveform, as shown in Fig. 8(a)-(i). Furthermore, the corresponding discharge current peaks are very small compared with those of the other gas flow rate conditions. In contrast, at the gas flow rates ranging from 300 to 500 sccm, the plasma plumes can

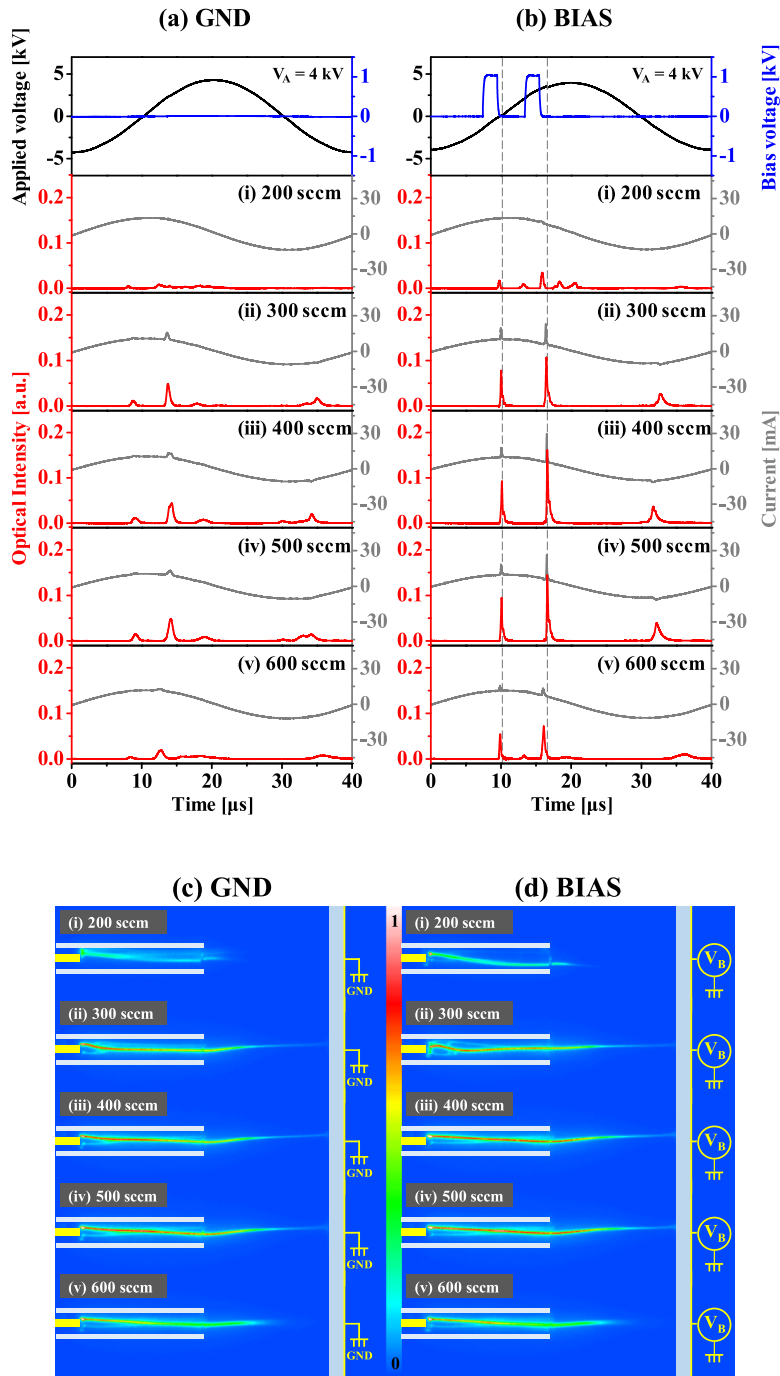


FIG. 8. Averaged waveforms of currents and optical emissions during 1000 periods relative to gas flow rate ranging from 200 to 600 sccm ((i) 200 sccm, (ii) 300 sccm, (iii) 400 sccm, (iv) 500 sccm, and (v) 600 sccm) when (a) is no bias (=ground) and (b) is pulse bias condition of Fig. 7(a)-(vi). Corresponding ICCD images measured during discharge produced under operating conditions without and with bias condition, where (c) is no bias condition of (a) and (d) is bias condition of (b). When using ICCD camera, exposure time of shutter is 40 ms and gain is 30 dB.

reach the ground counter electrode, as shown in Fig. 8(c)-(ii), (iii), and (iv), presumably due to the sufficient carrier gas supply toward surrounding air. In this case, the plasma plume can propagate from the jet head toward the ground counter electrode, thus forming a highly conductive channel between the starting and ending points.²¹ This conductive channel could enable the spatial distributions of

optical emissions and space charge to be gradually decreased toward the counter ground electrode. As a consequence, the optical emissions during the application of positive-going sinusoidal waveform are very high and also the optical emission during the application of one negative-going sinusoidal waveform can be observed, as shown in Fig. 8(a)-(ii), (iii), and (iv). The corresponding discharge current peaks are observed to increase considerably thanks to this conductive channel. However, at the gas flow rate of 600 sccm, the plasma plumes are observed to intermittently reach the ground counter electrode, as shown in Fig. 8(c)-(v). This phenomenon would be presumably due to the increased turbulence at the interface between the carrier gas and surrounding air. Thus the optical emissions and corresponding discharge current peaks became weaker and irregular during the whole period, as shown in Fig. 8(a)-(v).

When the proper bias pulse, *i.e.*, the bias pulse of Fig. 7(a)-(iv), is applied in Fig. 8(b), all the discharges during the whole period are observed to be stabilized considerably under the gas flow rates ranging from 300 to 500 sccm, as shown in Fig. 8(b)-(ii), (iii), and (iv). Like the cases of Fig. 8(c)-(ii), (iii), and (iv), the ICCD images of Fig. 8(d)-(ii), (iii), and (iv) also show that the proper gas flow rate condition could enable the plasma plumes to reach the biased counter electrode, and as such the application of the proper bias pulse to the counter electrode contributes to improving the spatial distribution and its intensity of the optical emissions in the space between the jet head and the counter electrode. When the same bias pulse, *i.e.*, the bias pulse of Fig. 7(a)-(iv), is applied at the gas flow rates of 200 and 500 sccm, the optical emissions of Fig. 8(b)-(i) and (v) during the application of the positive-going sinusoidal waveform seem to be a little narrow and increased, compared with the widely distributed optical emissions of Fig. 8(a)-(i) and (v) with no bias condition. Furthermore, the optical emissions during the application of the negative-going sinusoidal waveform show the poor characteristics, as shown in Fig. 8(b)-(i) and (v), which would be similar to those of Fig. 8(a)-(i) and (v) with no bias condition. In this case, the ICCD images also show almost the same feature as those of Fig. 8(a)-(i) and (v) with no bias condition. This experimental observation implies that it is very difficult to enhance the jet stability in the case of the gas flow condition in which the plasma plume cannot efficiently propagate toward surrounding air.

Optical emission spectroscopy is employed to investigate the changes of the resulting excited species in ambient air depending on whether the bias pulse is applied or not. In this case, the operating conditions, such as the distance between the jet tube and counter ground plate, gas flow rate, applied sinusoidal waveform, correspond to those of Fig. 8(a)-(iv), whereas the auxiliary bias pulse condition is exactly the same as that of Fig. 8(b)-(iv). Figures 9(a) and 9(b) show the optical emission spectra within the spectral range from 290 to 970 nm measured at the position of 4 mm apart from the jet head without and with auxiliary bias pulses, respectively. Comparing the overall spectrum of both cases, the overall spectra seem very similar except the difference in the emission intensities between without and with bias pulses. The increase in the optical emission intensity induced by an application of the proper bias pulse seems consistent with the ICCD discharge images of Fig. 8(d)-(ii), (iii), and (iv) measured under the proper gas flow rate condition.

In the spectral range from 300 to 450 nm, OH (at 308.8 nm) and N₂ lines (at 337.1, 357.6, 380.5, 408.8 nm) are identified in both conditions. The OH line is commonly produced by the dissociation process of H₂O molecules in ambient air or carrier gas and the N₂ lines are produced by excitation and accompanying transition to the different energy state of ground-state N₂. For the SW-APPJ, these dissociation and excitation processes commonly occur due to the energetic electrons and metastable species, which are supplied from jet head to surrounding air. In the spectral range from 690 to 860 nm, many strong Ar metastable (Ar_m) and O₂ (at 777.4 nm) lines are identified. In our jet condition, the active species such as electrons, Ar ions, and Ar metastable species are generated within the tube and diffused through surrounding air, thereby producing the excited species. Thus, the active and excited species generated in air are expected to show a strong spatial dependence from the jet head to the counter electrode. Figs. 9(c) and 9(d) show the spatial variations in the optical intensities of several species measured from the jet head to the counter electrode with an interval of 2 mm without and with bias pulse, respectively. For the spatial dependence of Ar lines (at 696.54, 763.51, 771.38 nm) in both conditions, the emission intensities of Ar metastable species are gradually decreased from the jet head toward the counter electrode. This experimental observation appears presumably associated with a reduction of the carrier gas concentration due to an increase in the distance from the jet head.

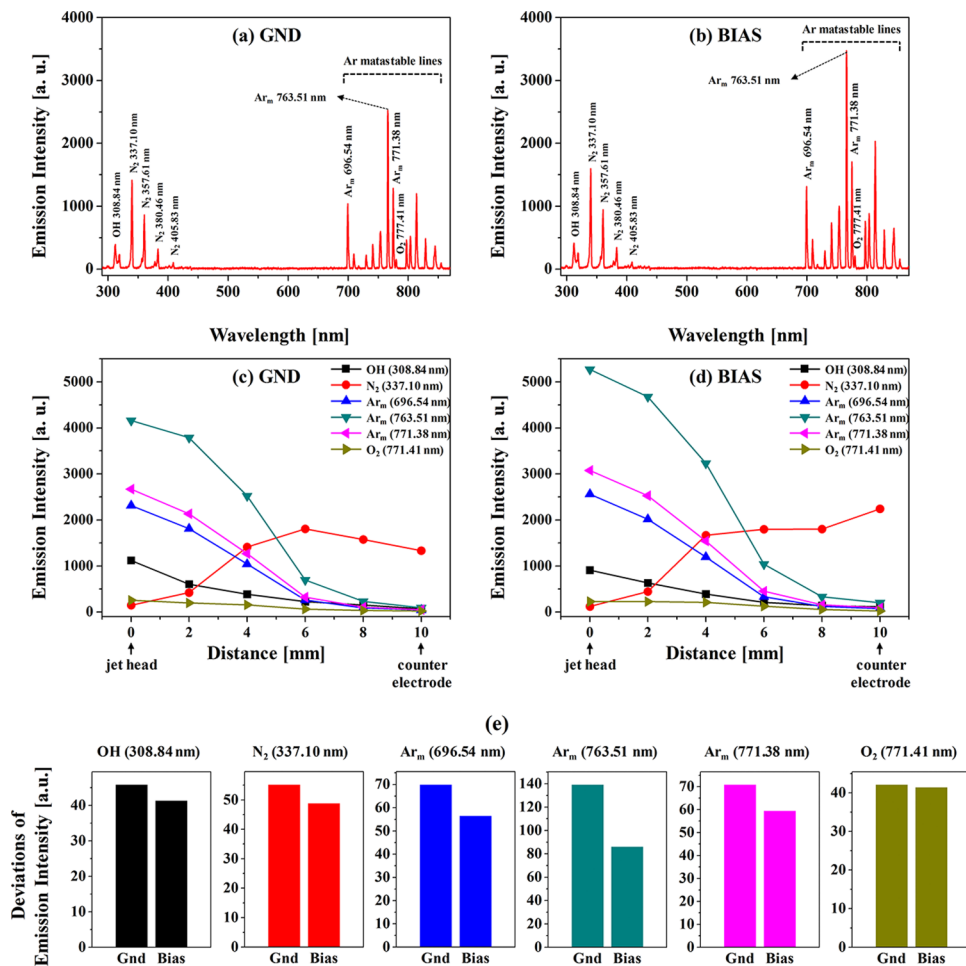


FIG. 9. Optical emission spectra within spectral range from 290 to 970 nm measured at position of 4 mm apart from jet head without (a) and with auxiliary bias pulses (b), spatial variations in optical intensities of several species such as OH, N₂, Ar, and O₂ measured from jet head to counter electrode with interval of 2 mm without (c) and with auxiliary bias pulse (d), and comparison (e) of standard deviations (SD) for successive 100 emission intensities of several species measured at position of 4 mm apart from jet head before and after application of auxiliary bias pulse.

As shown in Figs. 9(c) and 9(d), the emission intensities of Ar metastable species under the bias pulse are observed to be stronger than those under no bias condition at all measured points. In contrast, the emission intensity of N₂ line (at 337.10 nm) is increased with an increase in the distance from the jet head to 6 mm in both cases. This different tendency between the Ar and N₂ lines could result partly from the changes in concentration ratio of the Ar and air with respect to the distance, and also partly from the energy transfer through the penning reaction of N₂ with Ar metastable species ($N_2(X^1\Sigma_g^+) + Ar_m \rightarrow N_2(C^3\Pi_u^+) + Ar$). Furthermore, in the distance larger than 6 mm, the emission intensity of N₂ line begins to decrease slightly at no bias condition, *i.e.*, ground counter electrode, whereas the emission intensity of the N₂ line continuously increases at bias condition. For the emission intensity of the other excited species of OH (at 308.8) and O₂ line (at 771.4 nm) measured from 2 to 8 mm distance, both emission intensities of the bias counter electrode condition are observed to be slightly higher. Fig. 9(e) shows the comparison of the standard deviations (SD) for the successive 100 emission intensities of several species such as OH, N₂, Ar, and O₂ species measured at a position of 4 mm apart from the jet head, before and after application of the bias pulse. The successive 100 emission intensities are measured by fixing the exposure time at 4 ms (=100 periods) for each emission intensity. The SDs of all species are observed to be reduced at bias pulse condition, in particular, the SDs of Ar metastable species (at 696.5, 763.5, and 771.4 nm) are more reduced at bias pulse

condition, as shown in Figs. 9(e). These results imply that the auxiliary bias pulse contributing to initiating the discharges regularly could also contribute to stabilizing the production of the excited species in surrounding air, especially argon metastable species.

In summary, the proposed auxiliary bias pulse scheme cooperated with sinusoidal waveform can enhance the stability of the plasma emission for downstream surface treatments at atmospheric pressure without changes to the main atmospheric pressure plasma setup, such as a plasma device, the gas species, driving voltage and frequency, and their delicate and complex experimental correlation. Furthermore, in order to stabilize the SW-APPJs under the various process conditions, the auxiliary bias pulse scheme requires a precise adjustment of the bias pulse applied to the counter electrode, such that the stability of the SW-APPJs can be improved by adjusting the amplitude and number of the bias pulses based on the variations in the process conditions, such as the distance between the jet head and the counter electrode and the carrier gas flow rate.

IV. CONCLUSIONS

The instability of the SW-APPJs with combination of the dielectric barrier is deeply related to an inherent fluctuation of the accumulation of surface charges. In order to improve the stability of discharges, it is necessary to minimize the irregular discharges due to the fluctuation of the accumulation of surface charges. In this study, we have proposed the auxiliary bias pulse scheme to improve the stability of atmospheric pressure plasma jets driven by an AC sinusoidal waveform excitation source. When the auxiliary bias pulse is applied to the counter electrode, the gap voltage is reduced to suppress the irregular discharges. It should be noted that the stable discharge is produced when the auxiliary bias pulse is terminated. From the parametric study, such as the width, voltage, and onset time of auxiliary bias pulse, it has been demonstrated that the auxiliary bias pulse plays a significant role in suppressing the irregular discharges caused by the variation in memory voltage and stable discharge can be initiated with the termination of the auxiliary bias pulse. Furthermore, the careful experimental study on a precise adjustment of the bias pulse with respect to the various process conditions, confirms that the stability of the SW-APPJs can be improved by adjusting the amplitude and number of the bias pulses based on the variations in the process conditions, such as the distance between the jet head and the counter electrode and the carrier gas flow rate.

ACKNOWLEDGMENTS

This research was supported by Basic Science Research Program through the National Research Foundation of Korea (NRF) funded by the Ministry of Education (NRF-2013R1A1A4A03008577).

- ¹ J.Y. Kim, S.-O. Kim, Y. Wei, and J. Li, *Appl. Phys. Lett.* **96**, 203701 (2010).
- ² J.Y. Kim, J. Ballato, P. Foy, T. Hawkins, Y. Wei, J. Li, and S.-O. Kim, *Small* **6**, 1474 (2010).
- ³ J.Y. Kim, Y. Wei, J. Li, and S.-O. Kim, *Biosens. Bioelectron.* **26**, 555 (2010).
- ⁴ J.Y. Kim, Y. Wei, J. Li, P. Foy, T. Hawkins, J. Ballato, and S.-O. Kim, *Small* **7**, 2291 (2011).
- ⁵ J.Y. Kim, J. Ballato, P. Foy, T. Hawkins, Y. Wei, J. Li, and S.-O. Kim, *Biosens. Bioelectron.* **28**, 333 (2011).
- ⁶ J.Y. Kim, D. Lee, J. Ballato, W. Cao, and S. Kim, *Appl. Phys. Lett.* **101**, 224101 (2012).
- ⁷ D.Y. Kim, J.Y. Kim, H. Chang, M.S. Kim, J.-Y. Leem, J. Ballato, and S.-O. Kim, *Nanotechnology* **23**, 485606 (2012).
- ⁸ D.H. Kim, H.-J. Kim, C.-S. Park, B.J. Shin, J.H. Seo, and H.-S. Tae, *AIP Adv.* **5**, 097137 (2015).
- ⁹ C. Tendero, C. Tixier, P. Tristant, J. Desmaison, and P. Leprince, *Spectrosc. Acta Pt. B-Atom. Spectr.* **61**, 2 (2006).
- ¹⁰ M. Laroussi and T. Akan, *Plasma Process. Polym.* **4**, 777 (2007).
- ¹¹ X. Lu, M. Laroussi, and V. Puech, *Plasma Sources Sci. Technol.* **21**, 034005 (2012).
- ¹² Q. Bing, H. Jian-Jun, Z. Zhe-Huang, and W. De-Zhen, *Chin. Phys. Lett.* **25**, 3323 (2008).
- ¹³ J.L. Walsh, F. Iza, N.B. Janson, and M.G. Kong, *Plasma Sources Sci. Technol.* **21**, 034008 (2012).
- ¹⁴ J.L. Walsh, F. Iza, N.B. Janson, V.J. Law, and M.G. Kong, *J. Phys. D-Appl. Phys.* **43**, 075201 (2010).
- ¹⁵ Y.T. Zhang, D.Z. Wang, and M.G. Kong, *J. Appl. Phys.* **100**, 063304 (2006).
- ¹⁶ Y.H. Wang, Y.T. Zhang, D.Z. Wang, and M.G. Kong, *Appl. Phys. Lett.* **90**, 071501 (2007).
- ¹⁷ Y. Zhang, B. Gu, W. Wang, D. Wang, and X. Peng, *J. Appl. Phys.* **106**, 023307 (2009).
- ¹⁸ Y. Wang, H. Shi, J. Sun, and D. Wang, *Phys. Plasmas* **16**, 063507 (2009).
- ¹⁹ M.M. Becker, T. Hoder, R. Brandenburg, and D. Loffhagen, *J. Phys. D-Appl. Phys.* **46**, 355203 (2013).
- ²⁰ F.-C. Liu, Y.-F. He, and X.-F. Wang, *Chinese Phys. B* **23**, 075209 (2014).
- ²¹ H. Kim, A. Brockhaus, and J. Engemann, *Appl. Phys. Lett.* **95**, 211501 (2009).